Available online at website: https://journal.bcrec.id/index.php/bcrec

Bulletin of Chemical Reaction Engineering & Catalysis, 21 (1) 2026, 180-190

Original Research Article

Cold Plasma Modeling for Air Pollution Control: NOx Removal in Dielectric Barrier Discharge Reactors

Nesrine Labdouni*, Djilali Benyoucef, Hocine Tebani

Laboratory of Electrical Engineering and Renewable Energy (LGEER), Electrical Engineering Department, Faculty of Technology, Hassiba Benbouali University of Chlef, Algeria.

Received: 9th December 2025; Revised: 6th January 2026; Accepted: 7th January 2026
Available online: 15th January 2026; Published regularly: April 2026

Abstract

The paper presents a comprehensive numerical investigation of dielectric barrier discharges (DBDs) operating in atmospheric pressure air (N_2–O_2–Ar) containing NO concentrations between 2.5% and 10% is presented for plasma assisted NO_x mitigation. A one-dimensional fluid model is developed to describe the discharge dynamics and plasma chemical interactions under applied voltages of 8–12 kV and excitation frequencies of 2–4 kHz. The influence of voltage amplitude and frequency on electrical characteristics and NO_x removal efficiency is systematically analyzed. A representative operating condition (10% NO, 10 kV, 3 kHz) is examined in detail to elucidate the temporal evolution of voltage and current and the spatial distributions of electrons, ions, excited species, and neutral particles involved in NO dissociation pathways. The results provide improved insight into the reaction kinetics governing NO degradation in air plasma and offer practical guidance for optimizing DBD-based environmental remediation systems.

Keywords: Cold Plasma; Atmospheric Pressure; Nitrogen Oxides Reduction; Dielectric Barrier Discharge; Fluid Model

How to Cite: Labdouni, N., Benyoucef, D., Tebani, H. (2026). Cold Plasma Modeling for Air Pollution Control: NOx Removal in Dielectric Barrier Discharge Reactors. *Bulletin of Chemical Reaction Engineering & Catalysis*, 21 (1), 180-190. (DOI: 10.9767/bcrec.20560)

Permalink/DOI: https://doi.org/10.9767/bcrec.20560

1. Introduction

Atmospheric pollution has become a major global concern due to its impact on human health, climate, and environmental quality. Among the most critical pollutants, nitrogen oxides (NO_x) play a central role because of their involvement in photochemical smog, acid rain, ozone formation, and secondary particulate matter [1]. The two dominant species nitric oxide (NO) and nitrogen dioxide (NO_2) are primarily generated during high-temperature combustion, with NO representing nearly 95% of freshly emitted NO_x [2]. Despite being less toxic than NO_2, NO rapidly oxidizes in the atmosphere, contributing to harmful photochemical cycles. Major anthropogenic sources such as transportation, power generation, and industrial activities account for a large share of global NO_x effluent, making their mitigation an urgent priority [3].

Recently, Cold plasma systems have emerged as attractive substitutes for conventional approaches to NO_x reduction. These plasma-based processes rely on energetic electrons that trigger fast chemical reactions capable of decomposing or oxidizing NO_x at low temperatures [4]. Among the various NTP configurations, dielectric barrier discharges (DBDs) have gained specific interest thanks to their operational stability, flexibility, and ability to operate efficiently at atmospheric pressure [5]. A typical DBD consists of two electrodes spaced by at least one dielectric layer, which limits current and enables the generation of numerous transient micro discharges. This configuration has been widely applied in ozone generation, surface modification, environmental

* Corresponding Author.
Email: n.labdouni@univ-chlef.dz (N. Labdouni)

remediation, plasma-assisted combustion, excimer lamps, and other technological fields [6–8].

The efficiency of NO_x removal in plasma highly depends on the composition of the gas mixture, particularly N_2–O_2–Ar–NO systems. Electron impact processes generate a variety of reactive species excited atoms, radicals, ions, and meta stables that participate in NO dissociation and oxidation pathways [9]. A detailed comprehension of the interaction between discharge physics, plasma chemistry, and external operating parameters is therefore essential for optimizing DBD systems for pollutant abatement. Numerical modeling is a powerful approach to achieve this, providing detailed insight into plasma behavior under atmospheric-pressure conditions and complementing experimental studies [10].

Previous research on NO_x removal using DBDs has examined both standalone plasma reactors and hybrid plasma catalyst configurations. Studies have reported enhanced pollutant removal efficiencies under low-temperature conditions [11], investigated the effects of electrode geometry and dielectric materials [12], and demonstrated the role of oxygen concentration, hydrocarbon content, and discharge power in NO_x conversion [13–15]. Modeling efforts have further clarified the sensitivity of NO and N_2O formation to oxygen fraction and plasma power, with good agreement between simulations and experiments [16,17]. These contributions highlight the complex and highly condition-dependent nature of NO_x chemistry in non-thermal plasmas.

Motivated by these findings, the present work investigates the influence of voltage amplitude and frequency on the performance of a dielectric barrier discharge for NO reduction in atmospheric Air N_2–O_2–Ar–NO mixtures. Using a unidimensional fluid model, we explore the temporal extension of electrical parameters and the spatiotemporal behavior of electrons and reactive species responsible for NO decomposition. A representative mixture of 69% N_2, 20% O_2, 1% Ar, and 10% NO is examined in detail to elucidate relevant reaction pathways. The simulation results provide deeper insight into plasma-assisted NO conversion mechanisms and contribute to the optimization of DBD-based systems for environmental remediation and advanced plasma technologies.

2. Materials and Methods

2.1. Numerical Model

A fluid model in one dimensional was used to simulate the micro discharge behavior in a parallel-plate dielectric barrier discharge (DBD) reactor with a double dielectric layer. The simulations were performed using COMSOL Multiphysics, which solves the plasma transport equations self-consistently. The model couples Poisson's equation with the continuity, momentum, and energy equations for ions, electrons, and relevant neutral species. This approach enables time-resolved evaluation of the discharge current, applied voltage, electron density, electron temperature, and the spatial evolution of charged and neutral particles. The model captures the transient nature of micro discharges and provides a detailed description of plasma dynamics under different electrical operating conditions.

The governing equations follow the methodology presented in [18,19]:
Electron Transport: The electron density's continuity model is established using:

$$\frac{\partial n_e}{\partial t} + \nabla . \Gamma_e = R_e \quad (1)$$

$$\Gamma_e = -\mu_e E n_e - \nabla(D_e n_e) \quad (2)$$

Where, n_e represents the electron number density expressed in $(1/m^3)$, while R_e denotes the electron source term in $(1/m^3.s)$. The electron flux, Γ_e, accounts for electron transport due to drift and diffusion mechanisms. The drift component is governed by the electron mobility μ_e, expressed in $(m^2/V.s)$, in the presence of the electric field E, where E is given in (V/s). The diffusion contribution involves the electron diffusion coefficient D_e, expressed in (m^2/s), acting on the spatial gradient of the electron density. The symbol e refers to the electron species considered in the plasma discharge.
Electron energy is defined via:

$$\frac{\partial n_\varepsilon}{\partial t} + \nabla . \Gamma_\varepsilon + E . \Gamma_e = R_\varepsilon \quad (3)$$

$$\Gamma_\varepsilon = -\mu_\varepsilon E n_\varepsilon - \nabla(D_\varepsilon n_\varepsilon) \quad (4)$$

with n_ε denotes the electron energy density, expressed in (V/m^3). The term $R_\varepsilon$represents the source term associated with inelastic electron collisions, accounting for both energy gain and energy loss mechanisms due to interactions between electrons and neutral species, and is expressed in $(V/(m^3.s))$. The electron energy flux (Γ_e) includes contributions from drift and diffusion processes. The drift transport is controlled by the electron energy mobility μ_ε, expressed in $(m^2/V.s)$, under the influence of the electric field E. The diffusion term involves the electron energy diffusivity D_ε, expressed in (m^2/s), which governs the spatial redistribution of electron energy. The symbol ε refers to the electron energy considered in the plasma discharge. The energy of an electron, ε (V) calculated by:

$$\varepsilon = \frac{n_\varepsilon}{n_e} \quad (5)$$

Rate coefficients or Townsend coefficients are used to indicate the coefficients that originate from the above equations, depending on the system's molar concentration.

Assume that exist P collisions between inelastic electrons and neutrals and M processes that influence the increase or decrease of electron density. The energy loss of electron is calculated by:

$$R_e = \sum_{j=1}^{p} x_j k_j N_n n_e \Delta\varepsilon_j \quad (6)$$

where, is calculated as the sum of energy losses resulting from all inelastic collision processes between electrons and neutral species p. In this expression, the summation is performed over all inelastic reactions (j) involved in the plasma chemistry. The parameter x_j represents the mole fraction of the target neutral species participating in reaction (j), while k_j denotes the corresponding reaction rate coefficient expressed in j (m^3/s). The quantity N_n refers to the total neutral number density, expressed in ($1/m^3$), and accounts for the availability of collision partners in the discharge. The term $\Delta\varepsilon_j$ represents the energy loss associated with reaction (j), expressed in electron volts, which depends on the specific inelastic process such as excitation, ionization, or dissociation. This formulation allows the total electron energy loss to be evaluated self-consistently by summing the contributions of all relevant inelastic collision processes occurring in the plasma.

The mean electron energy (ε) has an exponential relationship with the Townsend coefficients (k_j). A function of the following kind can be used to fit the Townsend coefficients when a Maxwellian EEDF is assumed:

$$k_j = A\varepsilon^{\beta} e^{-E/\varepsilon} \quad (7)$$

Electrostatic Equations: The electrostatic field distribution is calculated through Poisson's equation, expressed as follows:

$$-\nabla.\varepsilon_0.\varepsilon_r \nabla V = \rho \quad (8)$$

where, V represents the electrostatic potential, ε_r is the relative permittivity, and ε_0 is the vacuum permittivity, and ρ corresponds to the space charge density. The space charge density (ρ) is calculated automatically based on the plasma chemistry defined in the model, using the following formula:

$$\rho = q(\sum_{k=1}^{N} Z_k n_k - n_e) \quad (9)$$

with Z_k represents the electric charge, q is the absolute terms of electronic charge. The constitutive relation given by:

$$D = \varepsilon_0 \varepsilon_r E \quad (10)$$

Submicroscopic characteristics of the coating medium that has dielectric feature and the relevant material properties are explained by relation (10) by connecting the electric field (E) and electric displacement (D). The following limiting condition adds to surface charge buildup to borders:

$$-n.(D_1 - D_2) = \rho_s \quad (11)$$

With ρ_s is the boundary's solution to the distributed ODE that follows:

$$\frac{d\rho_s}{dt} = n.J_i + n.J_e \quad (12)$$

With $n.J_i$ and $n.J_e$ are the wall's total current density of electron and total current density of ion are both represented by the normal component.

2.2 Chemical Model

2.2.1. Plasma model species:

The chemical kinetics of the Air–NO plasma mixture is highly complex. The model includes all nitrogen reactions listed in Supporting Information (Table S1) and all oxygen reactions in Table S2, along with more than 240 additional reactions involving nitrogen, oxygen, and argon species presented in Tables S3, S4 and S5. In total, the simulation tracks 34 plasma species presented in Table 1, including electrons, neutrals, ions, and excited states. These reactions cover key processes such as dissociation, ionization, recombination, excitation, and charge exchange. This comprehensive reaction set enables accurate modeling of the formation and depletion of reactive species, particularly those

Table 1. Plasma model species.

Neutral species	Positive species	Negative species	Exited species
N, O, O_3, NO, NO_2, NO_3, N_2O, N_2O_5	Ar^+, Ar_2^+, NO^+, NO_2^+, O_2^+, O^+, N_2^+	e^-, O^-, O_2^-, O_3^-, O_4^-, NO^-, NO_2^-	N_2(a1s), N_2(A3s), N_2(B3p), N_2(C3p), N(d), N(p), O(1d), O(1s), O_2(a1d), O_2(b1s), O_2(45), Ar(s)

influencing NO_x conversion, and ensures reliable prediction of plasma behavior under different electrical and gas-mixture conditions.

2.2.2. Ions mobilities

The electron mobility is computed based on electron-neutral collision cross sections, which are incorporated into the simulation through a Boltzmann solver or from validated experimental data [20]. In contrast, the ion mobilities for the gaseous mixtures studied in this work are determined using polarization theory. This approach allows the estimation of the reduced mobility of an ion through the following relation [21]:

$$\mu_m = \frac{36.10^{-4}}{\sqrt{\alpha.M_r}}.\frac{T}{T_0} \text{ in } (m^2/V.\ s) \quad (13)$$

$$M_r = \frac{m_i.m_n}{m_i+m_n} \quad (14)$$

The coefficient a denotes the polarizability of the neutral molecule, expressed in atomic units, and reflects the ability of the neutral species to be polarized by the electric field generated by the moving ion. The parameter M_r corresponds to the reduced mass of the ion neutral pair, also expressed in atomic units, and is calculated from the individual masses of the ion (m_i) and the neutral molecule (m_n) according to Equation (14), where the reduced mass represents the effective inertial contribution governing momentum transfer during collisions. The gas temperature T characterizes the thermal state of the background gas under operating conditions, while T_0 refers to the reference or initial temperature at which the reduced mobility is defined.

The mobility of charged species in the N_2–O_2–Ar–NO mixture was calculated using Blanc's law, which assumes additive momentum transfer collision frequencies in multicomponent gases. According to this formulation, the inverse mobility in the mixture, $\frac{1}{\mu_{Air/NO}}$, is obtained as the mole-fraction-weighted sum of the inverse mobilities in each pure gas component, i.e.:

$$\frac{1}{\mu_{Air/NO}} = \frac{F_{N_2}}{\mu_{N_2}} + \frac{F_{O_2}}{\mu_{O_2}} + \frac{F_{Ar}}{\mu_{Ar}} + \frac{F_{NO}}{\mu_{NO}} \quad (15)$$

where, F_i represents the mole fraction of species i, and μ_i denotes the mobility of the same charged particle in the pure gas i at the reference temperature and pressure. This approach provides an effective mobility for the mixture that accounts for the relative contributions of all background gases while preserving the physical influence of each component.

2.2.3 Chemical reactions of heavy species

The tables (S1-S5) display the reactions that produce and destroy the heavy species, along with the rate constants related to them. The Arrhenius equation [22] is used to quantitatively determine the rate coefficients k^f for the reactions that are utilized in our model token.

$$k^f = Ae^{E_a/RT} \quad (16)$$

while A is the pre-exponential factor that accounts for the frequency of effective molecular collisions and the steric characteristics of the reacting species. The exponential term incorporates the activation energy E_a, which represents the minimum energy barrier that must be overcome for the reaction to proceed and is expressed in units consistent with the product of the universal gas constant R and the absolute temperature (R^*T). The gas temperature T, expressed in kelvin, governs the thermal energy available to the reacting species, whereas R denotes the universal gas constant. All reaction sets for Nitrogen (N_2), Oxygen (O_2), Argon (Ar), and their mixtures are summarized in Tables (S1–S5) in the Supporting Information.

2.2.4 Surface reaction processes

Surface processes neutralize ions on dielectric surfaces and are characterized by a surface interaction coefficient, representing the probability of a species reacting upon contact. Mathematically, this defines the particle flux at the surface described in the following relation [41]:

$$\Gamma_k = \gamma_k n_k \sqrt{\frac{k_B T_k}{2\pi m_k}} \quad (17)$$

where the flux (Γ_k) corresponds to the number of particles of species k reaching the surface per unit area and time. This flux is proportional to the surface interaction coefficient (γ_k), which characterizes the efficiency of surface reactions, and to the number density (n_k) of the considered species in the gas phase. The thermal motion of the particles is taken into account through the square-root term, which depends on the Boltzmann constant (k_B), the temperature (T_k) of species k, and its mass (m_k). This expression accounts for the thermal motion of heavy species and the probability of reaction upon surface contact. The following interfacial reactions are implemented in (Table 2).

3. Results and Discussion

This section provides a detailed presentation of the simulation results describing the approach of the dielectric barrier discharge (DBD) plasma

in air mixture containing 69% N_2, 20% O_2, 1% Ar, and 10% NO at atmospheric pressure for NO removal. The DBD occurs under a sinusoidal voltage, with 3 cm × 3 cm parallel electrodes covered by a 0.635 mm thick dielectric ($\varepsilon_r = 9$). The 1 mm discharge gap operates at 10 kV peak voltage and 3 kHz frequency, starting from a 10% NO concentration. The DBD plasma cell geometry used in the simulation is shown in Figure 1.

3.1 Temporal Evolution of Electrical Parameters

Figure 2 presents the time-resolved evolution of the applied voltage and discharge current over a complete electrical cycle. The voltage exhibits a nearly sinusoidal waveform with peak values around ±10 kV, typical of a high-voltage AC signal. The current, however, is highly non-sinusoidal, displaying sharp transients and irregular oscillations between 0.1 mA and 0.9 mA, remaining positive throughout. This behavior arises from the modeling approach, where the discharge current represents only the conduction and displacement currents through the dielectric, both defined as positive in the simulation. The pronounced current spikes reflect rapid charge transfer events at the dielectric surface during the DBD process

3.2 Number Densities of Positive and Negative Charged Particles

Figures 3 and 4 illustrate the dynamic evolution of charged species during the DBD discharge. NO^+ dominates the positive ion population, reaching densities around 10^{17} m^{-3}, while lighter ions, such as O_2^+, N_2^+, and O^+, oscillate in the 10^{12}–10^{14} m^{-3} range. Rare gas ions

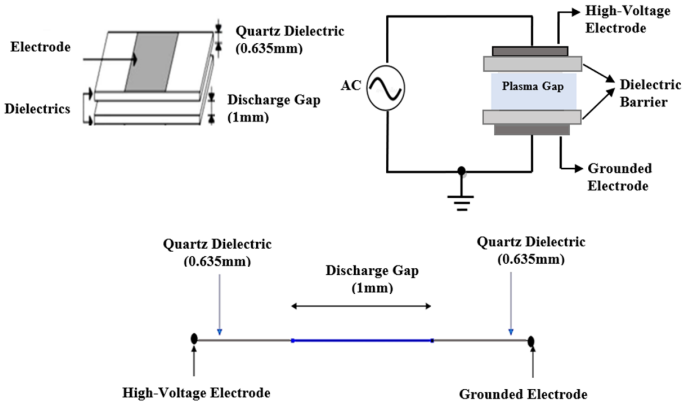

Figure 1. Configuration of DBD model geometry.

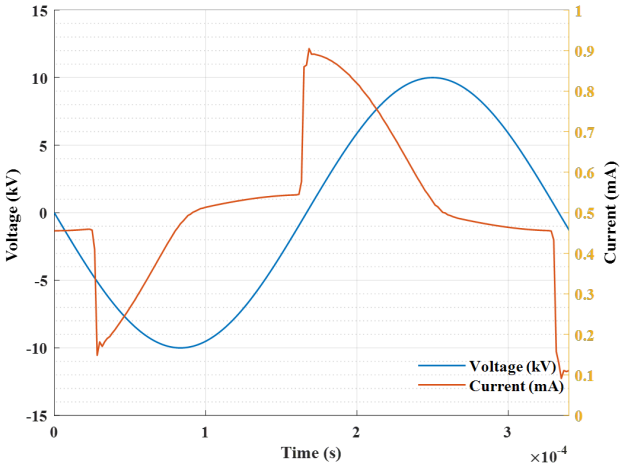

Figure 2. Discharge current and voltage waveform in DBD discharge.

Table 2. Interfacial reaction.

Reaction	Formula	Reaction	Formula
01	$N^+ \Rightarrow N$	21	$O(1d) \Rightarrow O$
02	$N_2^+ \Rightarrow N_2$	22	$O(1s) \Rightarrow O$
03	$N_3^+ \Rightarrow N_2+N$	23	$O_2(a1d) \Rightarrow O_2$
04	$N_4^+ \Rightarrow N_2+N_2$	24	$O_2(a1s) \Rightarrow O_2$
05	$N \Rightarrow 0.5N_2$	25	$O_2(b1s) \Rightarrow O_2$
06	$N(d) \Rightarrow N$	26	$O_2(45) \Rightarrow O_2$
07	$N(p) \Rightarrow N$	27	$O^+ \Rightarrow O$
08	$N_2(A) \Rightarrow N_2$	28	$O_2^+ \Rightarrow O_2$
09	$N_2(A3s) \Rightarrow N_2$	29	$O_3^+ \Rightarrow O_2+O$
10	$N_2(B3p) \Rightarrow N_2$	30	$O_4^+ \Rightarrow O_2+O_2$
11	$N_2(C3p) \Rightarrow N_2$	31	$O \Rightarrow 0.5O_2$
12	$N_2(a1s) \Rightarrow N_2$	32	$O^- \Rightarrow O$
13	$NO^+ \Rightarrow NO$	33	$O_2^- \Rightarrow O_2$
14	$NO^- \Rightarrow NO$	34	$O_3^- \Rightarrow O_2+O$
15	$NO_2 \Rightarrow O_2+N$	35	$O_4^- \Rightarrow O_2+O_2$
16	$NO_2^+ \Rightarrow O_2+N$	36	$NO_3^- \Rightarrow N+O_3$
17	$NO_2^- \Rightarrow N+O_2$	37	$N_2O^- \Rightarrow N_2O$
18	$NO_3^+ \Rightarrow O_3+N$	38	$Ar^+ \Rightarrow Ar$
19	$N_2O \Rightarrow O+N_2$	39	$Ar_2^+ \Rightarrow Ar+Ar$
20	$N_2O^+ \Rightarrow N_2O$	40	$Ar(s) \Rightarrow Ar$

(Ar^+, Ar_2^+) remain almost constant at much lower densities (~10^8 m^{-3}), reflecting their inertness. Electron densities closely follow the main molecular ions, highlighting the strong coupling between ionization and the applied voltage.

Among negative ions, NO_2^- and O^- are predominant (~10^{12} m^{-3}), while O_2^-, O_3^-, O_4^-, and NO^- also contribute, with their concentrations anti-correlated to electron density due to attachment processes. The periodic variations in both positive and negative species reveal the rapid ionization, attachment, and recombination events governed by the applied electric field. These results demonstrate a highly active plasma environment, emphasizing the intricate temporal chemistry and providing insights into the kinetics essential for optimizing plasma-based gas treatment.

3.3 Number Densities of Exited Particles

Figures 5 and 6 illustrate the temporal evolution of key excited species in the DBD plasma, providing insights into energy distribution and excitation kinetics. For nitrogen, long-lived metastable states, such as N_2(A3s), reach peak densities around 6×10^{13} m^{-3}, with sharp rises during each discharge pulse followed by exponential decay, while higher-energy states N_2(B3p) and N_2(C3p) exhibit similar but lower-density trends. These dynamics confirm nitrogen's central role in energy transfer, secondary ionization, and optical emission processes.

Excited oxygen species, including O(1s), O(1d), and O_2 (b1s, a1d, 45), show much higher peak densities, up to 10^{17} m^{-3}, with clear periodicity linked to the applied voltage, reflecting efficient electron-impact excitation. Excited argon species are less abundant (~10^{10} m^{-3}) but follow similar trends, potentially sustaining the plasma via Penning ionization. Overall, these results highlight the transient and voltage-synchronized nature of excitations, emphasizing oxygen's dominant contribution to reactive species and the complex interplay of excitation, quenching, and energy transfer in the plasma.

3.4 Number Densities of Neutral Particles during NO Removal in DBD

Figure 7 depicts the evolution of major neutral species relevant to NO removal in the

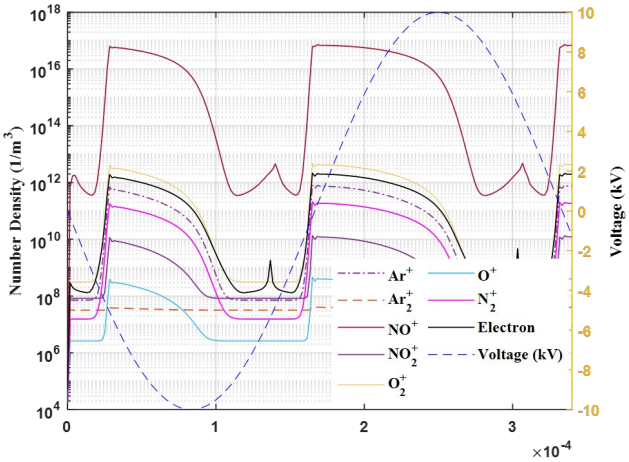

Figure 3. Evolution of positive charges densities in DBD discharge.

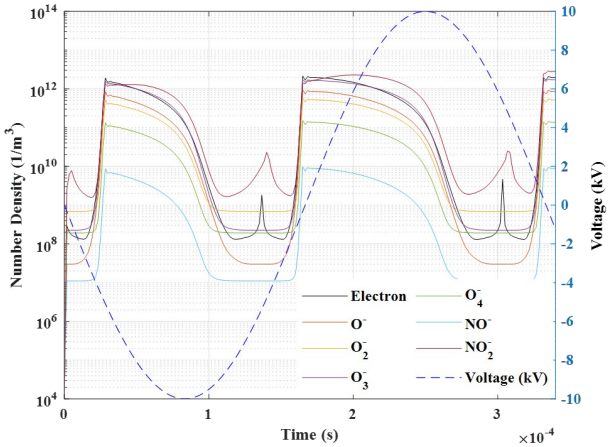

Figure 4. Evolution of negative charges densities in DBD discharge.

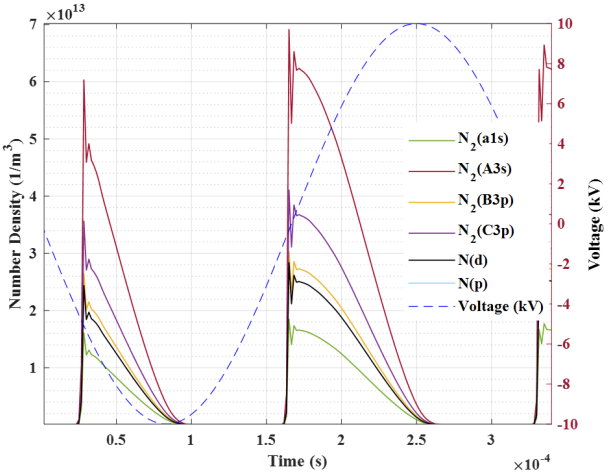

Figure 5. Evolution of excited nitrogen species densities in DBD discharge.

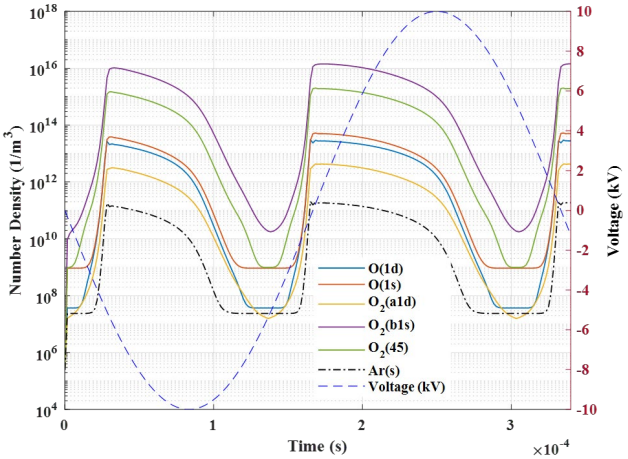

Figure 6. Evolution of excited oxygen species densities in DBD discharge.

DBD plasma across a 100 ms interval. The number densities are shown on a logarithmic scale (10^5–10^{25} m^{-3}) to capture their wide dynamic range. The most striking feature is the continuous decrease in NO concentration, starting from an initial value of approximately 10^{24} m^{-3} and dropping by several orders of magnitude throughout the simulation. This strong depletion reflects the efficiency of plasma-activated mechanisms, including reactions with O and N radicals and oxidation pathways that convert NO into higher nitrogen oxides.

Simultaneously, NO_2 forms rapidly and reaches a quasi-steady concentration around 10^{21} m^{-3}, indicating that the oxidation of NO to NO_2 dominates during the early discharge period. This behavior aligns with the classical reaction pathway:

$$NO + O \rightarrow NO_2 \quad (18)$$

As the discharge progresses, further oxidation leads to the formation of NO_3, N_2O_5, and O_3, which exhibit slower but steady increases in concentration. Notably: (a). NO_3 increases gradually and stabilizes near 10^{18} m^{-3}, indicating its role as a secondary oxidation product; (b). N_2O_5 and O_3 show delayed formation but reach similar concentrations, highlighting the multi-step reaction pathways involving NO_2 and O atoms or radicals; (c). N_2O forms rapidly and stabilizes early, reflecting the contribution of recombination and neutral-neutral reactions in the nitrogen cycle; (d). Atomic oxygen (O) and atomic nitrogen (N), although present in relatively low concentrations, show modest initial increases before reaching steady plateaus. These radicals serve as essential intermediates, initiating and sustaining the chain of reactions responsible for NO degradation; (e). Ozone emerges as one of the dominant oxidants in the latter phase of the discharge, achieving concentrations on the order of 10^{22} m^{-3}. Its presence is crucial not only for the oxidation of NO and NO_2, but also for the generation of higher oxides such as NO_3 and N_2O_5.

The temporal behavior of the species demonstrates that NO removal in DBD plasma is governed by an initial burst of fast radical-driven reactions, followed by slower oxidation and recombination processes leading to stable by-products. The interplay among NO, NO_2, O, O_3, and higher nitrogen oxides highlights the complexity of plasma chemical kinetics and underscores the importance of tuning plasma parameters to maximize pollutant removal while mitigating unwanted by-product formation.

3.5 Temporal Variation of NO Mole Fraction

Figure 8 presents the time-dependent variation of the NO mole fraction under various initial NO concentrations (10%, 7.5%, 5%, and 2.5%) in a DBD reactor. In all cases, the NO mole fraction decreases rapidly over time, confirming the effectiveness of plasma-assisted processes in reducing NO under atmospheric-pressure conditions. For the highest concentration (10% NO), the decline is most pronounced in the early stages, driven by intense interactions with energetic electrons and reactive particles such as oxygen atomic, ozone, and excited nitrogen. Notably, at approximately 0.025 seconds, more than 99% of the initial NO is removed in all cases, regardless of the starting concentration. This rapid depletion indicates that the DBD system achieves high removal efficiency within a very short residence time. Lower initial concentrations (e.g., 2.5% NO) show a more gradual decline, yet the total removal is still achieved within the same timeframe. This behavior highlights the nonlinear dependence of NO depletion kinetics on the initial concentration, which arises due to differences in reaction rates and species interactions.

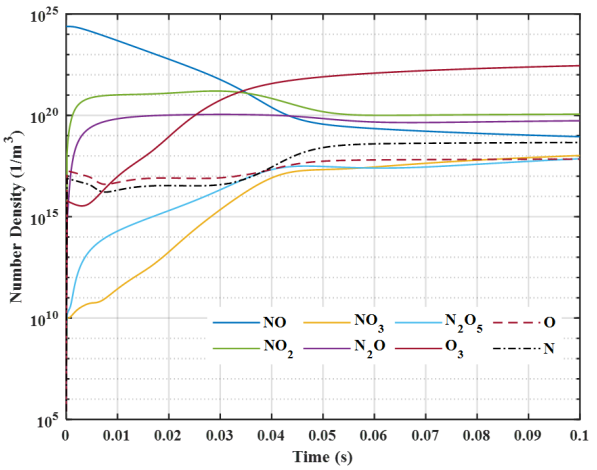

Figure 7. Evolution of neutral species during NO removal in DBD.

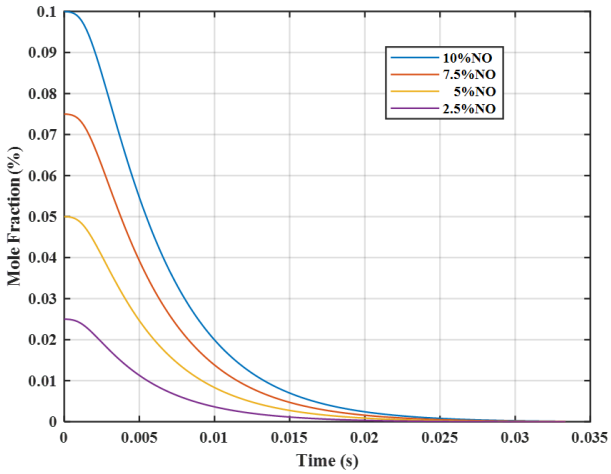

Figure 8. Temporal variation mole fractions of NO during 100 periods of DBD discharge.

Overall, the data validate the high reactivity and efficiency of the DBD plasma in removing NO. These findings can guide the optimization of reactor parameters, such as discharge power and residence time, for environmental applications targeting NO reduction.

3.6 Voltage-Frequency Effects on the NO Removal and Current Waveform

Figures 9 and 10 show how NO mole fractions and the corresponding current waveforms evolve over time under varying voltage and frequency conditions in the DBD reactor. In Figure 9, the effect of applied voltage is examined for 8 kV, 10 kV, and 12 kV at a fixed frequency of 3 kHz with an initial NO concentration of 10%. The findings show that rising the applied voltage markedly enhances NO removal efficiency. Higher voltages produce stronger electric fields, which accelerate electrons to higher energies, enabling more frequent dissociation and oxidation reactions of NO. This leads to the formation of reactive species such as O, O_3, and N, that play a fundamental role in NO decomposition.

The current waveform reflects this behavior: higher voltages generate sharper and more intense current peaks, indicating stronger micro discharges and increased electron-impact activity. At 0.025 s, the NO mole fraction drops significantly at all voltage levels, but the decline is most pronounced at 12 kV, confirming that intensified plasma activity accelerates NO conversion. In contrast, at 8 kV the removal rate is noticeably slower, suggesting that the available electron energy is insufficient to fully sustain the gas-phase chemistry within the short plasma residence time. Overall, these observations highlight the essential role of the applied voltage in controlling plasma strength and chemical reactivity in DBD-based NO_x abatement.

Figure 10 shows the influence of frequency on NO removal for 2 kHz, 3 kHz, and 4 kHz at a constant voltage of 10 kV. Increasing the frequency significantly boosts NO degradation. With higher frequencies, the number of discharge cycles per second increases, leading to more frequent electron-impact events and continuous formation of reactive species such as O, O_3, and excited N_2/O_2 states. These species accelerate NO oxidation and dissociation processes. The NO mole fraction at 0.025 s is lowest for 4 kHz, demonstrating faster and more efficient removal at higher discharge repetition rates. The current waveform becomes denser and more regular at elevated frequencies, reflecting improved discharge uniformity and higher average power density. This enhanced temporal continuity of micro discharges supports more effective plasma-driven chemical reactions. Thus, frequency acts as a key operational parameter that governs both plasma stability and chemical conversion efficiency in DBD reactors.

Collectively, the voltage–frequency analysis demonstrates a synergistic influence: increasing voltage strengthens the plasma and raises electron energy, while higher frequency increases the discharge repetition rate and reactive species generation. Both factors work together to improve NO removal performance.

4. Conclusion

This study provides a detailed analysis of NO_x behavior and removal in a DBD reactor operating in atmospheric Air–NO_x mixtures. Through a fluid model in one-dimensional, we investigated the spatiotemporal transition of charged particles, excited particles, and neutral molecules under different electrical conditions. The results confirm that DBD reactors efficiently promote NO_x decomposition via electron-impact reactions and the generation of reactive species such as atomic oxygen (O), ozone (O_3), and excited nitrogen and oxygen states. The NO mole fraction decreases rapidly over time, with the strongest reduction

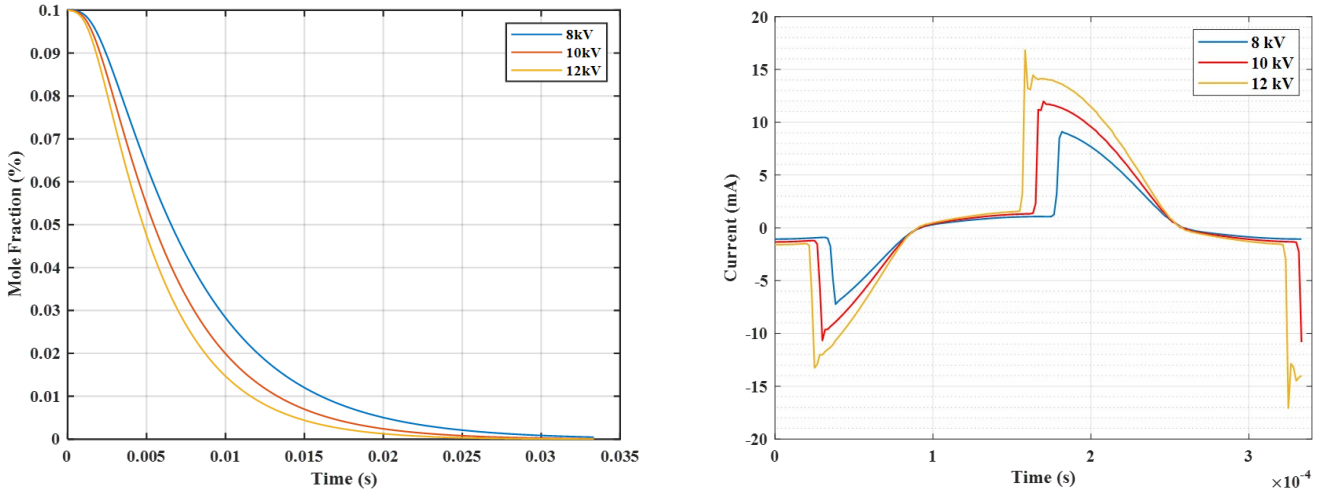

Figure 9. Effect of voltage on the NO removal and current waveform in DBD discharge.

occurring at higher applied voltages and frequencies. This improvement is directly linked to enhanced electron energy and increased discharge repetition, which intensify plasma-induced chemical pathways. The analysis of species densities further clarifies the underlying plasma chemistry, confirming the formation of essential intermediates and secondary products. Additionally, the study highlights the sensitivity of NO removal to initial concentration, voltage, and frequency, emphasizing the necessity of optimizing these parameters for effective pollution control. Future work should focus on: Experimental validation of the simulated trends to strengthen the reliability of the model; Multi-dimensional and time-resolved modeling to capture spatial non-uniformities, streamer behavior, and electrode effects; Energy-efficiency optimization, including improved reactor geometry, electrode design, and power delivery systems; Scaling-up studies for integration into real industrial exhaust treatment systems. Overall, the outcomes of this study highlight the potential of DBD reactors as an efficient non-thermal plasma technology for NO_x mitigation and provide a roadmap for future improvements and practical implementation.

Acknowledgment

The authors gratefully recognize the Laboratory of Electrical Engineering and Renewable Energy (LGEER), Faculty of Technology, Hassiba Benbouali University of Chlef, for its continuous support and the research infrastructure that made this study possible.

CRedit Author Statement

Author Contributions: Nesrine Labdouni: Conceptualization, Methodology, Investigation, Software, Data Curation, Visualization Writing Original Draft; Djilali Benyoucef: Supervision, Project Administration, Writing Review and Editing, Validation, Resources; Hocine Tebani: Co-supervision, Writing Review and Editing, Validation. All authors have read and agreed to the published version of the manuscript.

References

[1] Fayyazbakhsh, A., Bell, M.L., Zhu, X., Mei, X., Koutný, M., Hajinajaf, N., Zhang, Y. (2022). Engine emissions with air pollutants and greenhouse gases and their control technologies. *Journal of Cleaner Production*, 376, 134260. DOI: 10.1016/j.jclepro.2022.134260

[2] Bruggeman, P.J., Iza, F., Brandenburg, R. (2017). Foundations of atmospheric pressure non-equilibrium plasmas. *Plasma Sources Science and Technology*, 26(12), 123002. DOI; 10.1088/1361-6595/aa97af.

[3] Talebizadeh, P., Babaie, M., Brown, R., Rahimzadeh, H., Ristovski, Z., Arai, M. (2014). The role of non-thermal plasma technique in NOx treatment: A review. *Renewable and Sustainable Energy Reviews*, 40, 886-901. DOI: 10.1016/j.rser.2014.07.194.

[4] Skalska, K., Miller, J.S., Ledakowicz, S. (2010). Trends in NOx abatement: A review. *Science of the Total Environment*, 408(19), 3976-3989. DOI: 10.1016/j.scitotenv.2010.06.001.

[5] Babaie, M., Davari, P., Talebizadeh, P., Ristovski, Z., Rahimzadeh, H., Brown, R. (2013). Study of particulate matter removal mechanism by using non-thermal plasma technology. In *Proceedings of the XIII International Conference on Electrostatic Precipitation (pp. 1-7). International Society for Electrostatic Precipitation (ISESP).* https://eprints.qut.edu.au/60837/

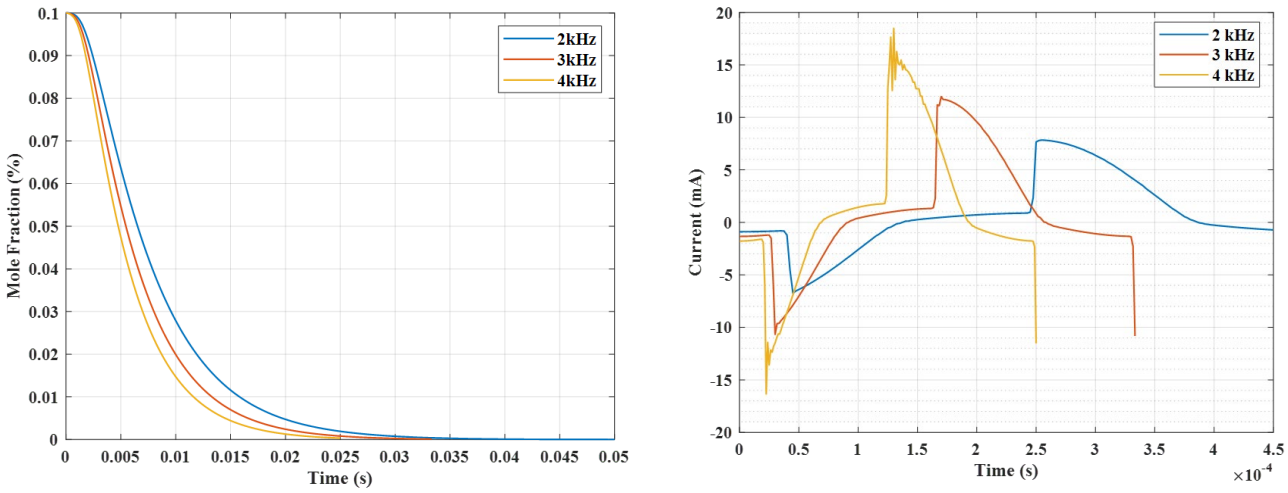

Figure 10. Effect of frequency on the NO removal and current waveform in DBD discharge.

[6] Ghomi, H., Safa, N.N., Ghasemi, S. (2011). Investigation on a DBD plasma reactor. *IEEE Transactions on Plasma Science*, 39(11), 2104-2105. DOI: 10.1109/tps.2011.2160735.

[7] Fang, Z., Lin, J., Yang, H., Qiu, Y., Kuffel, E. (2009). Polyethylene terephthalate surface modification by filamentary and homogeneous dielectric barrier discharges in air. *IEEE Transactions on Plasma Science*, 37(5), 659-667. DOI: 10.1109/TPS.2009.2015322.

[8] Lahouel, M.H., Benyoucef, D., tebani, H. (2021). Modeling and parametric study of dielectric barrier discharge in pure nitrogen at atmospheric pressure. *Turkish Journal of Physics*, 45(1), 26-42. DOI: 10.3906/fiz-2003-5 .

[9] Jolibois, J., Takashima, K., Mizuno, A. (2012). Application of a non-thermal surface plasma discharge in wet condition for gas exhaust treatment: NOx removal. *Journal of Electrostatics*, 70(3), 300-308. DOI: 10.1016/j.elstat.2012.03.011.

[10] Mohapatro, S., Rajanikanth, B.S. (2011). Study of pulsed plasma in a crossed flow dielectric barrier discharge reactor for improvement of NOx removal in raw diesel engine exhaust. *Plasma Science and Technology*, 13(1), 82. DOI: 10.1088/1009-0630/13/1/17.

[11] Matsumoto, T., Wang, D., Namihira, T., Akiyama, H. (2010). Energy efficiency improvement of nitric oxide treatment using nanosecond pulsed discharge. *IEEE Transactions on Plasma Science*, 38(10), 2639-2643. DOI: 10.1109/TPS.2010.2045903

[12] Anaghizi, S.J., Talebizadeh, P., Rahimzadeh, H., Ghomi, H. (2015). The configuration effects of electrode on the performance of dielectric barrier discharge reactor for NOx removal. *IEEE Transactions on Plasma Science*, 43(6), 1944-1953. DOI: 10.1109/TPS.2015.2422779.

[13] Cai, Y., Lu, L., Li, P. (2020). Study on the effect of structure parameters on NO oxidation in DBD reactor under oxygen-enriched condition. *Applied Sciences*, 10(19), 6766. DOI: 10.3390/app10196766

[14] Qiao, J.J., Yang, Q., Wang, L.C., Albrechts, M.C.K., Tsonev, I., Bogaerts, A., Xiong, Q. (2025). Kinetics of N2 vibrational excitation and NO formation in nanosecond-pulsed air discharge: Can vibrational-translational nonequilibrium be exploited for efficient N2 fixation, *Plasma Sources Science and Technology*. 34 065008. DOI: 10.1088/1361-6595/ade33c

[15] Paulauskas, R., Jõgi, I., Striūgas, N., Martuzevičius, D., Erme, K., Raud, J., Tichonovas, M. (2019). Application of non-thermal plasma for NOx reduction in the flue gases. *Energies*, 12(20), 3955. DOI: 10.3390/en12203955

[16] Silva, T., Bera, S., Pintassilgo, C.D., Herrmann, A., Welzel, S., Tsampas, M.N., ... Guerra, V. (2024). Unraveling NO Production in N2–O2 Plasmas with 0D Kinetic Modeling and Experimental Validation. *The Journal of Physical Chemistry A*, 128(34), 7235-7256. DOI: 10.1021/acs.jpca.4c03323

[17] Okubo, M., Yamada, H., Yoshida, K., Kuroki, T. (2017). Simultaneous reduction of diesel particulate and NOx using a catalysis-combined nonthermal plasma reactor. *IEEE Transactions on Industry Applications*, 53(6), 5875-5882. DOI: 10.1109/TIA.2017.2748925

[18] Amine, N.Y.M., Mohamed, M., Djilali, B. (2025). Investigation of Ar/CH_4 Mixtures in Dielectric Barrier Discharge: A Simulation Approach for Hydrogen Production. *Bulletin of Chemical Reaction Engineering & Catalysis*, 20(3), 458-470. DOI: 10.9767/bcrec.20352.

[19] Chenoui, M., Tebani, H., Benyoucef, D. (2026). Modeling and Electrical Characterization of CO_2/Ar Dielectric Barrier Discharges at Atmospheric Pressure. *Bulletin of Chemical Reaction Engineering & Catalysis*, 21(1), 38-50. DOI: 10.9767/bcrec.20493.

[20] Parent, B., Rodriguez Fuentes, F.M. (2024). Progress in electron energy modeling for plasma flows and discharges. *Physics of Fluids*, 36(8). DOI: 10.1063/5.0219552

[21] Carbone, E., Graef, W., Hagelaar, G., Boer, D., Hopkins, M. M., Stephens, J. C., ... Pitchford, L. (2021). Data needs for modeling low-temperature non-equilibrium plasmas: the LXCat project, history, perspectives and a tutorial. *Atoms*, 9(1), 16. DOI: 10.3390/atoms9010016

[22] Lahouel, M.H.A., Benyoucef, D., Gadoum, A. (2023). One Dimensional Modeling of Dielectric Barrier Discharge in Pure Oxygen at Atmospheric Pressure Using Comsol Multiphysics. *ArXiv Preprint*, arXiv:2302.13813. DOI: 10.48550/arXiv.2302.13813

[23] Cheng, K.W., Hung, C.T., Lin, K.M., Chiu, Y.M., Wu, J.S., Yu, J.P. (2012). Fluid modeling of a nitrogen atmospheric-pressure planar dielectric barrier discharge driven by a realistic distorted sinusoidal alternating current power source. *Japanese Journal of Applied Physics*, 51(11R), 116001. DOI: 10.1143/JJAP.51.116001

[24] Massines, F., Segur, P., Gherardi, N., Khamphan, C., Ricard, A. (2003). Physics and chemistry in a glow dielectric barrier discharge at atmospheric pressure: diagnostics and modelling. *Surface and Coatings Technology*, 174, 8-14. DOI: 10.1016/S0257-8972(03)00540-1.

[25] Triniti Database, www.lxcat.net, retrieved on May 4, 2025

[26] Bacri, J., Medani, A. (1980). Electron diatomic molecule weighted total cross section calculation. *Physica B+C*, 101(3), 399-409. DOI: 10.1016/0378-4363(80)90037-6

[27] Lazarou, C., Koukounis, D., Chiper, A.S., Costin, C., Topala, I., Georghiou, G.E. (2015). Numerical modeling of the effect of the level of nitrogen impurities in a helium parallel plate dielectric barrier discharge. *Plasma Sources Science and Technology*, 24(3), 035012. DOI: 10.1088/0963-0252/24/3/035012

[28] Tsai, I.H., Hsu, C.C. (2010). Numerical simulation of downstream kinetics of an atmospheric-pressure nitrogen plasma jet. *IEEE Transactions on Plasma Science*, 38(12), 3387-3392. DOI: 10.1109/TPS.2010.2084598

[29] Choi, Y.H., Kim, J.H., Hwang, Y.S. (2006). One-dimensional discharge simulation of nitrogen DBD atmospheric pressure plasma. *Thin Solid Films*, 506, 389-395. DOI: 10.1016/j.tsf.2005.08.103

[30] Phelps Database, www.lxcat.net, retrieved on May 4, 2025

[31] Kossyi, I.A., Kostinsky, A.Y., Matveyev, A.A., Silakov, V.P. (1992). Kinetic scheme of the non-equilibrium discharge in nitrogen-oxygen mixtures. *Plasma Sources Science and Technology*, 1(3), 207. DOI: 10.1088/0963-0252/1/3/011

[32] Morgan Database, www.lxcat.net, retrieved on May 4, 2025

[33] Lefkowitz, J.K., Guo, P., Rousso, A., Ju, Y. (2015). Species and temperature measurements of methane oxidation in a nanosecond repetitively pulsed discharge. *Philosophical Transactions of the Royal Society A: Mathematical, Physical and Engineering Sciences*, 373(2048), 20140333. DOI: 10.1098/rsta.2014.0333

[34] Hayashi Database, www.lxcat.net, retrieved on May 4, 2025

[35] Eichwald, O., Yousfi, M., Hennad, A., Benabdessadok, M.D. (1997). Coupling of chemical kinetics, gas dynamics, and charged particle kinetics models for the analysis of NO reduction from flue gases. *Journal of Applied Physics*, 82(10), 4781-4794. DOI: 10.1063/1.366336

[36] Lahouel, M.H.A. (2021). Modélisation et simulation d'une décharge à barrière diélectrique dans un mélange gazeux à la pression atmosphérique. *Doctoral Dissertation*. Hassiba Benbouali University of Chlef, supervised by D. Benyoucef & H. Tebani. Retrieved from http://hdl.handle.net/123456789/1642.

[37] Mokhtaria, Benyamina. (2014). Etude de la production de l'ozone dans les décharges couronne. *Université d'Offrandes Sciences et de la Technologie (USTOMB)*.

[38] Vichiansan, N., Leksakul, K., Chaopaisarn, P., Boonyawan, D. (2021). Simulation of simple 2D plasma jet model for NO, OH, and H2O2 production via Multiphysics in laminar flow and transport of diluted species through design of experiment method. *AIP Advances*, 11(3). DOI: 10.1063/5.0044611

[39] SIGLO Database, www.lxcat.net, retrieved on May 4, 2025

[40] Liu, D., Sun, B., Iza, F., Xu, D., Wang, X., Rong, M., Kong, M.G. (2017). Main species and chemical pathways in cold atmospheric-pressure Ar+ H2O plasmas. *Plasma Sources Science and Technology*, 26(4), 045009. DOI: 10.1088/1361-6595/aa5c22

[41] Baadj, S., Larouci, B., Belasri, A., Pontiga, F., Benmoussa, A., Saidia, L. (2023). Chemical and Electrical Aspects of Homogeneous Discharge in an Argon-Oxygen Mixture for Ozone Generation. *Plasma Medicine*, 13(4). DOI: 10.1615/PlasmaMed.2024052657.